To further confirm such an assertion, we have deposited Cu_3Ge onto n^+-ZnSe and n-ZnSe to see if we can indeed achieve p^+-n^+ and p^+-n junction-like I-V characteristics. In these cases, we carried out an extra 200 nm mesa etch with an area of $220 \times 100\ \mu m^2$ after Cu_3Ge/Pt/Au was deposited onto the n^+-ZnSe or n-ZnSe surface. Ti/Pt/Au, a well known material for realising ohmic contacts to n^+-ZnSe and n-ZnSe, was subsequently deposited onto the etched surface.

Fig. 2 shows the room-temperature I-V characteristics of the Cu_3Ge contact to n^+-ZnSe and n-ZnSe. These I-V curves were measured by applying an external voltage across the upper Cu_3Ge/Pt/Au contact and the Ti/Pt/Au ohmic contact. It can be seen that when Cu_3Ge was deposited onto n-ZnSe, a p^+-n junction-like I-V characteristic was achieved. Under reverse bias (i.e. a lower voltage is applied on the Cu_3Ge/Pt/Au contact side and a higher voltage on the Ti/Pt/Au contact side), electrons at the degenerated valence band in the p^+ region can tunnel across the p^+-n junction which results in a large reverse bias current. The large > 10V forward turn-on voltage is probably due to the large ohmic contact resistance between Ti/Pt/Au and n-ZnSe. Under forward bias, we also observed a strong ZnSe bandgap related to the blue-green electroluminescence from the sample. The observed p^+-n junction-like I-V characteristic suggests that a Cu_3Ge contact could locally convert n-ZnSe into p^+-ZnSe so as to form a p^+-n junction in the sample.

The I-V characteristic of the Cu_3Ge contact to n^+-ZnSe was also shown in Fig. 2. It can be seen that we can observe a negative differential resistance (NDR) with a peak-to-valley ratio of ~6 under forward bias. Such NDR behaviour is very similar to that of conventional p^+-n^+ Esaki diodes. The fact that the Cu_3Ge contact to n^+-ZnSe results in an I-V characteristic very similar to that of a p^+-n^+ Esaki diode again suggests that Cu_3Ge can form a local p^+ region on the ZnSe surface. Such an observation also agrees well with the ohmic contact behaviour seen when Cu_3Ge is deposited onto p-ZnSe, as previously shown in Fig. 1.

In summary, Cu_3Ge/Pt/Au has been deposited on top of p-ZnSe, n^+-ZnSe and n-ZnSe. It was found that the observed Cu_3Ge/p-ZnSe ohmic behaviour is due mainly to hole tunnelling through the metal/semiconductor interface. Also, a p^+-n junction-like I-V characteristic was observed from Cu_3Ge/n-ZnSe. Furthermore, a negative differential resistance with a peak-to-valley ratio of ~6 was observed under forward bias when Cu_3Ge was deposited onto n^+-ZnSe. These observations all suggest that Cu_3Ge can form a local p^+ region on the ZnSe surface.

Acknowledgment: The authors would like to thank R.C. Tu for his assistance in MBE growth. This work is supported by the National Science Council, Rebublic of China, under contract number: NSC-88-2215-E-006-005.

11 October 1999
Electronics Letters Online No: 19991480
DOI: 10.1049/el:19991480

S.J. Chang, W.R. Chen, Y.K. Su and J.F. Chen (*Department of Electrical Engineering, National Cheng Kung University, Tainan, Taiwan 70101, Republic of China*)

W.H. Lan, A.C.H. Lin and H. Chang (*Chung Shan Institute of Science and Technology, Lung-Tan, Taiwan 325, Republic of China*)

References

1 FAN, Y., HAN, J., HE, L., SARAIE, J., GUNSHOR, R.L., HAGEROTT, M., JEON, H., NURMIKKO, V., HUA, G.C., and OTSUKA, N.: 'Graded band gap ohmic contact to p-ZnSe', *Appl. Phys. Lett.*, 1992, **61**, pp. 3160–3162

2 MENSZ, P.M.: 'BeTe/ZnSe graded band gap ohmic contacts to p-ZnSe', *Appl. Phys. Lett.*, 1994, **64**, pp. 2148–2150

3 DANDREA, R.G., and DUKE, C.B.: 'Design of ohmic contacts to p-ZnSe', *Appl. Phys. Lett.*, 1994, **64**, pp. 2145–2147

4 HIEI, F., IKEDA, M., OZAWA, M., MIYAJIMA, T., ISHIBASHI, A., and AKIMOTO, K.: 'Ohmic contacts to p-ZnSe using ZnTe/ZnSe multiquantum wells', *Electron. Lett.*, 1993, **29**, (10), pp. 878–879

5 KIJIMA, S., OKUYAMA, H., SANAKA, Y., KOBAYASHI, T., and TOMIYA, S.: 'Optimized ZnSe:N/ZnTe:N contact structure of ZnSe-based II-VI laser diodes', *Appl. Phys. Lett.*, 1998, **73**, (2), pp. 235–237

6 CHANG, S.J., CHEN, W.R., SU, Y.K., TU, R.C., LAN, W.H., and CHANG, H.: 'Ohmic contact to p-ZnSe and p-ZnMgSSe', *Electron. Lett.*, 1999, **35**, (15), pp. 1280–1281

Ultrasonic surface profile determination by spatial voting

B. Barshan

A novel spatial voting scheme is described for surface profile determination based on multiple ultrasonic range measurements. The approach is extremely robust, flexible and straightforward. It can deal with arbitrary numbers and sensor configurations, with the intrinsic ability to suppress spurious readings, crosstalk, and higher-order reflections, and process multiple reflections informatively.

Introduction: Ultrasonic sensors have been widely used in intelligent systems since they are robust, light and inexpensive. They are capable of revealing a great amount of useful information when coupled with appropriate data processing and interpretation. The approach described here is aimed at the determination of arbitrary surface profiles, and is completely novel in that a spatial voting scheme is applied to range data. Although voting strategies have been previously used in other areas [1 – 3] this is their first application to ultrasonic surface profile determination. The method presented is extremely flexible and can easily handle arbitrary sensor configurations as well as synthetic arrays obtained by moving a relatively small number of sensors. Approaches based on geometrical or analytical modelling are often limited to elementary target types or simple sensor configurations [4, 5]. A commonly noted disadvantage of ultrasonic range sensors is the difficulty associated with interpreting spurious readings, crosstalk, higher-order and multiple reflections. The proposed method is capable of effectively suppressing the first three of these, and has the intrinsic ability to process echoes returning from surface features further away than the nearest (i.e. multiple reflections) informatively.

The method presented in this Letter, which is based on the use of multiple ultrasonic range measurements combined with spatial voting and thresholding, can be applied to different physical modalities of range sensing of vastly different scales and in many different areas. These may include radar, sonar, optical sensing and metrology, remote sensing, ocean surface exploration, geophysical exploration, robotics and acoustic microscopy.

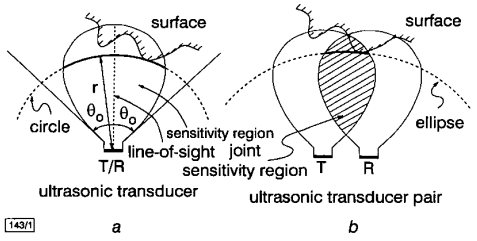

Fig. 1 *Arcs showing reflection points*

a For the same transducer transmitting and receiving (circular arc)
b For different transducers transmitting and receiving (elliptical arc)

Simple ultrasonic range sensors are considered that measure time-of-flight t_o, which is the round-trip travel time of the pulse between the transducer and the point of reflection. Given the speed of sound c, the range r can be easily calculated from $r = ct_o/2$. Although such devices return accurate range data, typically they cannot provide direct information on the angular position of the point on the surface from which the reflection was obtained. Thus, all that is known is that the reflection point lies on a circular arc of radius r, as illustrated in Fig. 1*a*. More generally, when one transducer transmits and another receives, it is known that the reflection point lies on the arc of an ellipse whose focal points are the transmitting and receiving elements (Fig. 1*b*). The arcs are tangential to the reflecting surface at the actual point(s) of reflection.

Most commonly, the large beamwidth of the transducer is accepted as a device limitation that determines the angular resolving power of the system, and the reflection point is assumed to be along the line of sight. In our method, circular or elliptical arcs representing the uncertainty of the object location are drawn. By combining the information inherent in a large number of such arcs, angular resolution far exceeding the beamwidth is obtained.

Surface profile determination: Structured sensor configurations such as linear and circular arrays, as well as irregularly configured, moving and synthetic arrays, have been considered. Structured arrays are often preferred in theoretical work for simplicity and ease of analysis, whereas the method presented here can cope with irregular arrays equally easily. Although the problem of optimal sensor placement is a subject for future research, the large number of simulations and experiments performed indicate that it is preferable to work with irregular arrays, since the randomised vantage points of the sensors tend to complement each other better than structured ones. As an illustrative example, Fig. 2*a* shows the arc map obtained from a surface using an irregular sensor configuration. Although each arc represents considerable uncertainty as to the angular position of the reflection point, the actual curve can be visually extracted by examining the arc map in Fig. 1*a*. Arc segments near the actual reflection points tend to reinforce each other. Arc segments not actually corresponding to any reflections and simply representing the angular uncertainty of the transducers remain more sparse and isolated. Similarly, those arcs caused by higher-order reflections, crosstalk and noise also remain sparse and lack reinforcement.

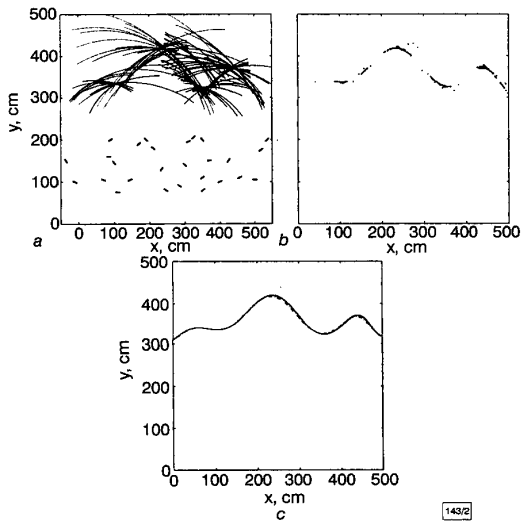

Fig. 2 *Arc map and sensor configuration, processed map and curve fit*

a Arc map and sensor configuration
b Processed map with $\tau = 5$
c Curve fitted to *b* and actual surface
——— curve fitted to *b*
– – – – actual surface: $\varepsilon = 2.74$cm

The information contained in the arc map is processed by employing a spatial voting scheme followed by thresholding. First, a matrix is created which represents the number of arcs crossing each pixel. The values of pixels that have not been crossed by any arcs remain zero. The values of other pixels are equal to the number of arcs crossing them. A pixel size of 1cm was used in our examples.

Next, a suitable threshold level τ is chosen to select those pixels that have been crossed more frequently. If the number of crossings for a given pixel is less than τ, the value of that pixel is set equal to zero. If the number is greater than or equal to τ, the pixel value is set equal to one.

The result of applying the above procedure to Fig. 2*a* is presented in Fig. 2*b*.

As a last step, a least-squares polynomial fit is obtained to compactly represent the surface. The curve fitted to the processed map in Fig. 2*b* is displayed in Fig. 2*c*. A root-mean-square error measure, $\varepsilon = \{N^{-1} \sum_{i=1}^{N} [p(x_i) - y(x_i)]^2\}^{1/2}$, comparing the fitted polynomial $p(x_i)$ with the actual surface profile $y(x_i)$, is introduced. Here, N is the total number of columns in the arc map matrix.

According to this criterion, the best result for the example of Fig. 2 is obtained with $\tau = 5$, as shown in Fig. 2*c*. The large number of simulations and experiments performed indicate that the minimum error is almost always obtained with threshold values between 4 and 6.

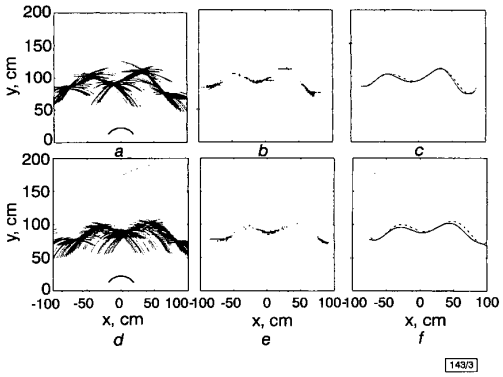

Fig. 3 *Arc maps, processed maps and curve fits*

a Arc map and sensor configuration
Data are collected by translating circular array of five sensors from (–75, 0) to (75, 0) and refiring every 2.5cm
b Processed map with $\tau = 5$
c ——— curve fitted to *b*
– – – – actual surface: $\varepsilon = 2.12$cm
d Arc map obtained from rough surface
e Processed map with $\tau = 5$
f ——— curve fitted to *e*
– – – – actual surface: $\varepsilon = 3.45$cm

Another example, based on experimentally obtained ultrasonic range data, is shown in Fig. 3*a–c*. Although the method was initially developed and demonstrated for specularly (mirror-like) reflecting surfaces, subsequent tests were performed also with Lambertian surfaces of varying roughness. The results indicate that the method still works for rough surfaces with slightly larger errors, as exemplified by Fig. 3*d–f*. The surface in Fig. 3*a–c* was made of smooth, thin cardboard, whereas the results in Fig. 3*d–f* were obtained when the same surface was covered with bubbled packing material. The ultrasonic devices used in the experiments were Polaroid 6500 series transducers, operating at a resonance frequency of $f_o = 49.4$kHz.

Conclusion: A novel method has been described for determining arbitrary surface profiles by applying spatial voting and subsequent thresholding to data acquired by ultrasonic range sensors. The method is extremely flexible, versatile and robust, as well as being simple and straightforward. It can deal with arbitrary numbers and configurations of actual and synthetic arrays of sensors. Accuracy improves with the number of sensors used and can be as low as a few centimetres. The method is robust in many aspects; it has the inherent ability to eliminate undesired range readings arising from higher-order reflections, crosstalk, and noise, as well as processing multiple echoes informatively.

The CPU times involved were of the order of a quarter of a second, indicating that the method is viable for real-time applications. Map-processing operations were implemented in the C programming language and the programs are run on a 200MHz Pentium Pro PC. The method can be readily generalised to three-dimensional environments with the arcs replaced by spherical or elliptical caps and the spatial voting rules extended to three dimensions. In certain problems, it may be preferable to reformulate the method using polar or spherical co-ordinates. Some applications may involve an inhomogeneous and/or anisotropic medium of propagation. It is envisioned that the method can be generalised to such cases by constructing broken or non-ellipsoidal arcs.

26 October 1999
Electronics Letters Online No: 19991477
DOI: 10.1049/el:19991477

B. Barshan (*Department of Electrical Engineering, Bilkent University, Bilkent, 06533 Ankara, Turkey*)

References

1 PARHAMI, B.: 'Voting algorithms', *IEEE Trans. Reliab.*, 1994, **43**, (4), pp. 617–629

2 LAM, L., and SUEN, C.Y.: 'Application of majority voting to pattern recognition: an analysis of its behavior and performance', *IEEE Trans. Syst. Man Cybern.*, 1997, **27**, (5), pp. 553–568

3 UTETE, S.W., BARSHAN, B., and AYRULU, B.: 'Voting as validation in robot programming', *Int. J. Robot. Res.*, 1999, **18**, (4), pp. 401–413

4 BROWN, M.K.: 'The extraction of curved surface features with generic range sensors', *Int. J. Robot. Res.*, 1986, **5**, (1), pp. 3–18

5 BARSHAN, B., and KUC, R.: 'Differentiating sonar reflections from corners and planes by employing an intelligent sensor', *IEEE Trans. Pattern Anal. Mach. Intell.*, 1990, **12**, (6), pp. 560–569

Erratum

WILSON, L.R., KEIGHTLEY, P.T., COCKBURN, J.W., SKOLNICK, M.S., CLARK, J.C., HILL, G., GREY, R., and HOPKINSON, M.: 'Comparison of performance of GaAs-AlGaAs and InGaAs-AlInAs quantum cascade lasers', *Electron. Lett.*, **35**, (23), pp. 2034–2036

Editor's corrections

In the third line of the abstract, 'InGaAs-Almas laser' should read 'InGaAs-AlInAs laser'.

In the first line of the first paragraph, 'InGaAs-MINAS' should read 'InGaAs-AlInAs'.

ESTIMATION OF LENGTH FOR *ELECTRONICS LETTERS* VERSION 5.1

As set by our typesetters, the maximum length in print of a Letter is 83 column cms, or three columns of about 27cms height. When judging the length of a submission, please take into account:

Title	0.5 column cm per 40 characters (or part thereof)
Abstract	1 column cm per 165 characters
Authors	1 column cm per separate affiliation
Text	1 column cm per 165 characters (it is easiest to estimate the number of characters, including spaces, per line and the number of lines per page)
References	1 column cm each
Tables	0.4 column cm per line
Figures	All figures are reduced to a width of 8.6cm. If the figure is wider than it is high, divide the height by the width and multiply by 8.6 column cm. If the figure is higher than it is wide (discouraged), the figure will occupy more than 8.6 column cm.
Captions	1 column cm per main figure or table caption (provided it is brief), 0.33 column cm per line for subcaptions (including keys and other information that will be removed from the figures).

Equations

Single line equations:	0.6–0.8	column cm per line
Integrals:	1.0	column cm per line
Quotients:	0.7–1.2	column cm per line
Sums and products:	1.2	column cm per line
Matrices:	0.4	column cm per line

For other equation types, refer to a recent issue of *Electronics Letters*. Excessively long equations will be split into several lines.